Optical and Quantum Electronics (2024) 56:1097
https://doi.org/10.1007/s11082-024-07046-7

DFT analysis of the electronic, optical, phonon, elastic, and mechanical features of ternary Rb_2XS_3 (X = Si, Ge, Sn) chalcogenides

Şule Uğur[1] · Melek Güler[2] · Alptuğ Özdemir[1] · Emre Güler[2] · Gökay Uğur[1]

Received: 12 March 2024 / Accepted: 1 May 2024
© The Author(s) 2024

Abstract
Density functional theory (DFT) calculations were executed for the titled features of hitherto unreported Rb_2XS_3 (X = Si, Ge, Sn) chalcogen compounds. All compounds were found to be in semiconducting character where they demonstrate high-k dielectric properties, high optical conductivity, high refractivity and reasonable absorbance. In addition, obtained phonon dispersion curves of all compounds with positive phonon frequencies stipulate the dynamical stability. Also, computed elastic stiffness constants prove mechanical stability and bilateral agreement between Pugh ratio analyses with Poisson ratio results confirms the ductile mechanical feature of all addressed compounds. Overall, with satisfactory optical, elastic and mechanical aspects, Rb_2XS_3 (X = Si, Ge, Sn) chalcogenides can be promising materials for recent optoelectronics and microelectronics with diverse applications.

Keywords Ternary · Chalcogen · Elastic · Electronic · Optical

1 Introduction

Ternary semiconducting chalcogenides are three-element materials that often include one or more chalcogens such as sulfur, selenium, or tellurium coupled with other elements, i.e., metals or metalloids (Sujith et al. 2022; Jawad et al. 2024; Azam et al. 2019). These compounds have drawn much attention because of their distinct electrical, optical, and sometimes magnetic characteristics, making them ideal choices for several technological applications (Hoang and Mahanti 2016; Mbilo and Musembi 2022; Kormath et al. 2018; McKeever et al. 2023; Shen et al. 2023; Wang et al. 2022). They are intensively researched for use in electronics, optoelectronics, and energy-related sectors like photovoltaics and thermoelectric devices. Further, each ternary chalcogenide has diverse features and possible uses, and ongoing scientific works investigate their potential in different innovative technology sectors. Among the

✉ Şule Uğur
suleugur@gazi.edu.tr

[1] Department of Physics, Faculty of Science, Gazi University, 06500 Ankara, Turkey

[2] Department of Physics, Ankara Hacı Bayram Veli University, 06900 Ankara, Turkey

Published online: 20 May 2024

ternary semiconducting chalcogenides, the family with the formula A_2BX_3 (A = Li, Na, K, Rb, Cs, and Cu with 1 + cation; B = Ti, Zr, C, Si, Ge, Sn, Pb with 4 + cation and X = O, S and Se with 2-anion) has become especially popular during the past half-decade due to their switchable polarizations like solid-state ferroelectrics and antiferroelectrics which make them functional materials for recent solar energy applications (Gorai et al. 2019; Khan et al. 2022). On the other hand, although several experimental and theoretical works were overlooked for the diverse physical viewpoints of A_2BX_3 ternary sulfur chalcogens, e.g., Na_2CS_3, Cu_2SiS_3, K_2TiS_3 (Bennett 2020) and Cs_2ZrS_3, Rb_2ZrS_3 (Khan et al. 2022), there is still not any theoretical work reported for the Rb_2XS_3 (X = Si, Ge, Sn) ternary sulfur chalcogens. Therefore, in this work, we have performed DFT calculations not only to answer the questionable electronic, elastic, mechanical, phonon, and optic features of Rb_2XS_3 (X = Si, Ge, Sn) compounds but also contribute to the future experimental and theoretical literature of these technologically crucial ternary sulfur chalcogens.

2 Computational concept

CASTEP plane-wave DFT code was handled (Clark et al. 2005; Segall et al. 2002, 1996) for all computations. Figure 1a–c indicates the crystal views of presently examined Rb_2XS_3 (X = Si, Ge, Sn) chalcogens under the symmetry of C2/M (C2H-3) with accompanying space group number 12. Further, Table 1. lists the lattice information of Rb_2XS_3 (X = Si, Ge, Sn) compounds with existing literature results. The generalized-gradient approximation (GGA) of DFT within the Perdew-Burke-Ernzerhof (PBE) exchange correlation was applied carefully (Perdew et al. 1996, 1998). A robust BFGS optimization algorithm (Güler and Güler 2013) was effectually applied to the alloys to reduce the constraints of geometry optimization procedures. For the electron–ion interactions of the studied compounds, OTFG-norm conserving pseudopotentials (Lejaeghere et al. 2013) were selected within Rb: [$5s^1$], Si: [$3s^2 3p^2$], Ge: [$3d^{10} 4s^2 4p^2$], Sn: [$4d^{10} 5s^2 5p^2$] and S: [$3s^2\ 3p^4$] the pseudo atomic configurations. The limit for energy cut-off was 600 eV for all compounds. Also, sampling of the Brillouin zone was done with the Monkhorst–Pack standard (Monkhorst and Pack 1976) with 3 × 5 × 4 k points. The converged energy limit was 5×10^{-6} eV/atom, whereas the maximum Hellmann–Feynman force value was kept at 0.01 eV/Å with an SCF tolerance of 5×10^{-6} eV/atom. During computations, displacements between the atoms were set to be 5×10^{-4} Å, where the atoms were exposed 0.02 GPa to external stress values. To resolve the optical characteristics, the highest incident energy was counted as 25 eV, which covers the infrared region (IR < 1.59 eV), visible (1.65–3.26 eV) scale, and the ultraviolet fragments (~4–123 eV) of the entire electromagnetic spectrum under [100] polarization vector. Dynamical stabilities were enlightened from the phonon dispersions of each compound from the linear response method, where elastic constants calculations were derived from the stress–strain method implemented in the CASTEP (Clark et al. 2005; Segall et al. 2002, 1996).

3 Results and discussion

3.1 Comparing the electronic bands of Rb_2XS_3 (X = Si, Ge, Sn) compounds

Figures 2, 3, and 4 portray each computed electronic band structure of Rb_2XS_3 (X = Si, Ge, Sn) compounds, with matching total density of states (TDOS) and partial density of states

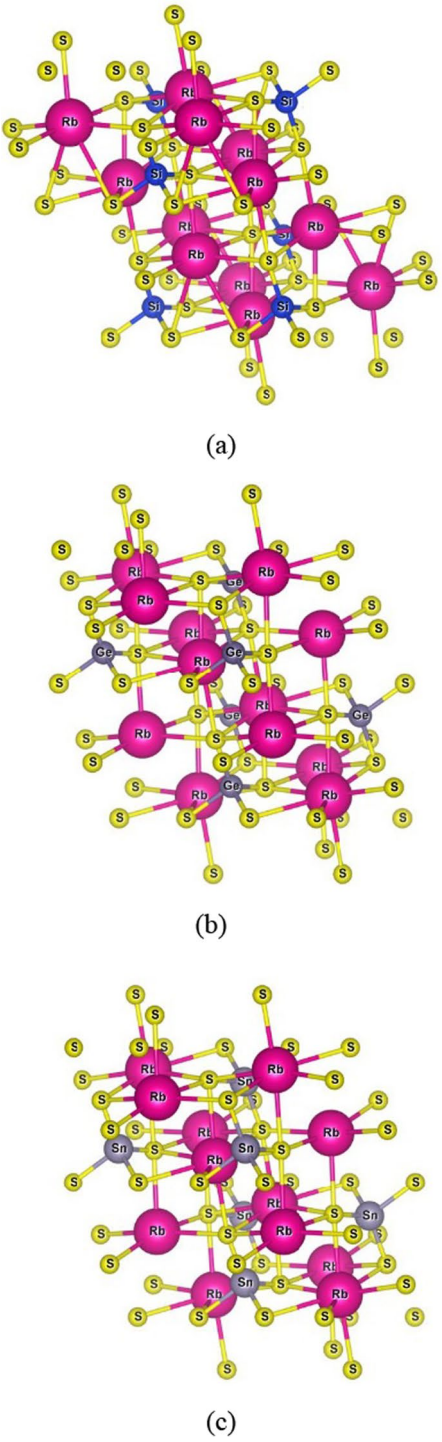


Fig. 1 Crystal views of Rb_2SiS_3 (**a**), Rb_2GeS_3 (**b**), and Rb_2SnS_3 (**c**) along with the y-axis

Table 1 Lattice information of Rb_2XS_3 (X = Si, Ge, Sn)

Chalcogen	Literature	*a* (Å)	*b* (Å)	*c* (Å)	*β*
Rb_2SiS_3	This work	13.568	6.961	9.812	134.521
	Jain et al. 2013) [Theor]	13.330	6.900	9.610	125.320
	Kirklin et al. (2015) [Theor]	13.445	6.926	9.673	125.598
Rb_2GeS_3	This work	13.798	7.015	9.919	125.724
	Jain et al. (2013) [Theor]	13.540	6.950	9.710	125.220
	Kirklin et al. (2015) [Theor]	13.684	6.985	9.801	125.566
Rb_2SnS_3	This work	14.364	7.143	10.087	126.035
	Kirklin et al. (2015) [Theor]	14.226	7.074	10.064	125.911

(PDOS) distributions, respectively. As is feasible within all band plots, Rb_2XS_3 (X = Si, Ge, Sn) compounds forbidden energy band gap formations peculiar to the semiconductors arise amongst the top edge of the valance bands (VB) and the bottom edge of the conduction bands (CB) of the considered compounds. Again, from Figs. 2, 3, and 4, all the band gaps display a direct nature where their values hold at 2.806 eV for Rb_2SiS_3, 2.206 eV for Rb_2GeS_3, and 2.156 eV for Rb_2SnS_3, around Fermi energy (E_F) levels those set to zero. In other words, the direct band gap order of Rb_2XS_3 (X = Si, Ge, Sn) compounds follows the $Rb_2SiS_3 > Rb_2GeS_3 > Rb_2SnS_3$ range. Further, all PDOS curves for each Rb_2XS_3 (X = Si, Ge, Sn) compound suggest the dominant contributions of the p-orbitals to the existing semiconducting behavior of these compounds where the p orbital of Rb_2SnS_3 has the highest contribution compared to Rb_2SiS_3 and Rb_2GeS_3.

3.2 Computed optical parameters for Rb_2XS_3 (X = Si, Ge, Sn) compounds

For recent technology, comprehensive evaluation of the optical properties is significant to produce novel optoelectronic devices. So, we concentrated on several distinct optical features of the examined compounds, i.e., optical absorptions, reflections, dielectric constants, refractions, photo conductivities, and loss functions. By the way, if a material is exposed to an outer energy of incident photons, the optical response of this material can be ascertained from the frequency-dependent Kramers–Kronig rule of $\varepsilon(\omega) = \varepsilon_1(\omega) + i\varepsilon_2(\omega)$. Here, $\varepsilon_1(\omega)$ indicates the real part (Re) that is sensible to energy storages, and $i\varepsilon_2(\omega)$ denotes the imaginary part (Im) of the complex dielectric function $\varepsilon(\omega)$ associated with the energy loss (Uğur et al. 2022; Güler et al. 2021a, 2021b, 2021c, 2023a). Also, the Kramers–Kronig rule allows us to attain other critical optical factors, i.e., optical absorption constants, reflection characteristics, refractivity indexes, and loss function (Bellil et al. 2021; Güler et al. 2021d, 2023b; Baaziz et al. 2022; Uğur et al. 2021a).

Figures 5, 6, and 7 demonstrate the obtained optical factors of Rb_2XS_3 (X = Si, Ge, Sn) compounds via the considered incident photon energy. In Fig. 5, all $\varepsilon_1(\omega)$ parts of surveyed Rb_2XS_3 (X = Si, Ge, Sn) compounds, which also determines the refractive of these compounds, begin over the scalar magnitude 6 and are identical to each other with little peaking differences. Due to their approaching limit of high-k dielectrics ($\varepsilon_1(\omega) > 7$) and overestimating limit of low-k dielectrics ($\varepsilon_1(\omega) < 3.9$), all Rb_2XS_3 (X = Si, Ge, Sn) compounds can be readily considered as high-k dielectric replacement materials of recent silicon dioxide gate dielectric materials often used in modern semiconductor manufacturing and many practical fields of microelectronics (Bellil et al. 2021; Güler et al. 2021d, 2023b; Baaziz

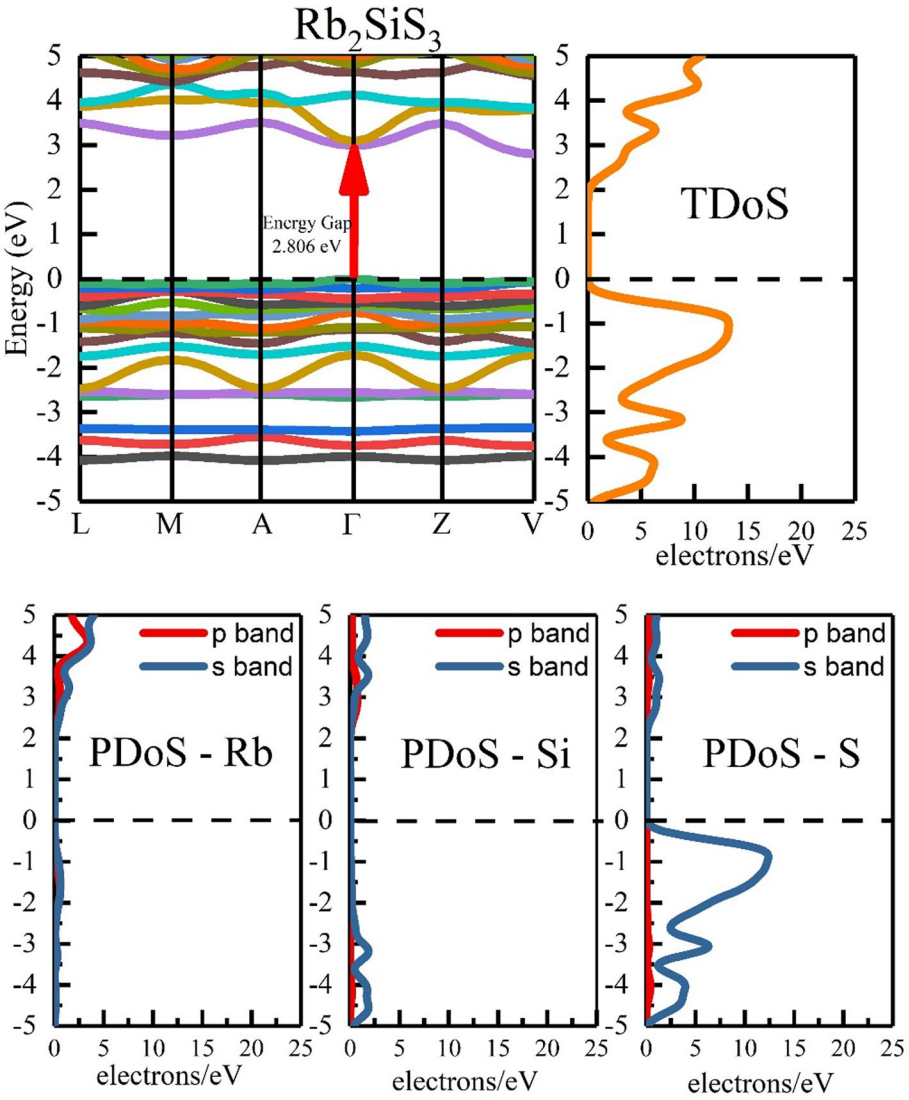


Fig. 2 Electronic band structure, total density of states, and partial density of state of Rb_2SiS_3

et al. 2022; Uğur et al. 2021a). Also, all Im parts of Rb_2XS_3 (X = Si, Ge, Sn) compounds signified with $\varepsilon_2(\omega)$ those cooperated to the optical absorption response initiates from zero energy values and track a similar photon energy raise, and then drop to zero energy points around 25 eV where they further stick to the unity.

The optical conductivity (photo-conductivity) expressed with σ (ω) signifies and implies the existence of thermal conduction in the presence of sufficient incoming photon energy (Bellil et al. 2021; Güler et al. 2021d, 2023b; Baaziz et al. 2022; Uğur et al. 2021a). In Fig. 6, the Rb_2XS_3 (X = Si, Ge, Sn) compounds display robust optical conductivities. Also, both real (Re) and Im (imaginary) components of Rb_2XS_3 (X = Si, Ge, Sn) compounds

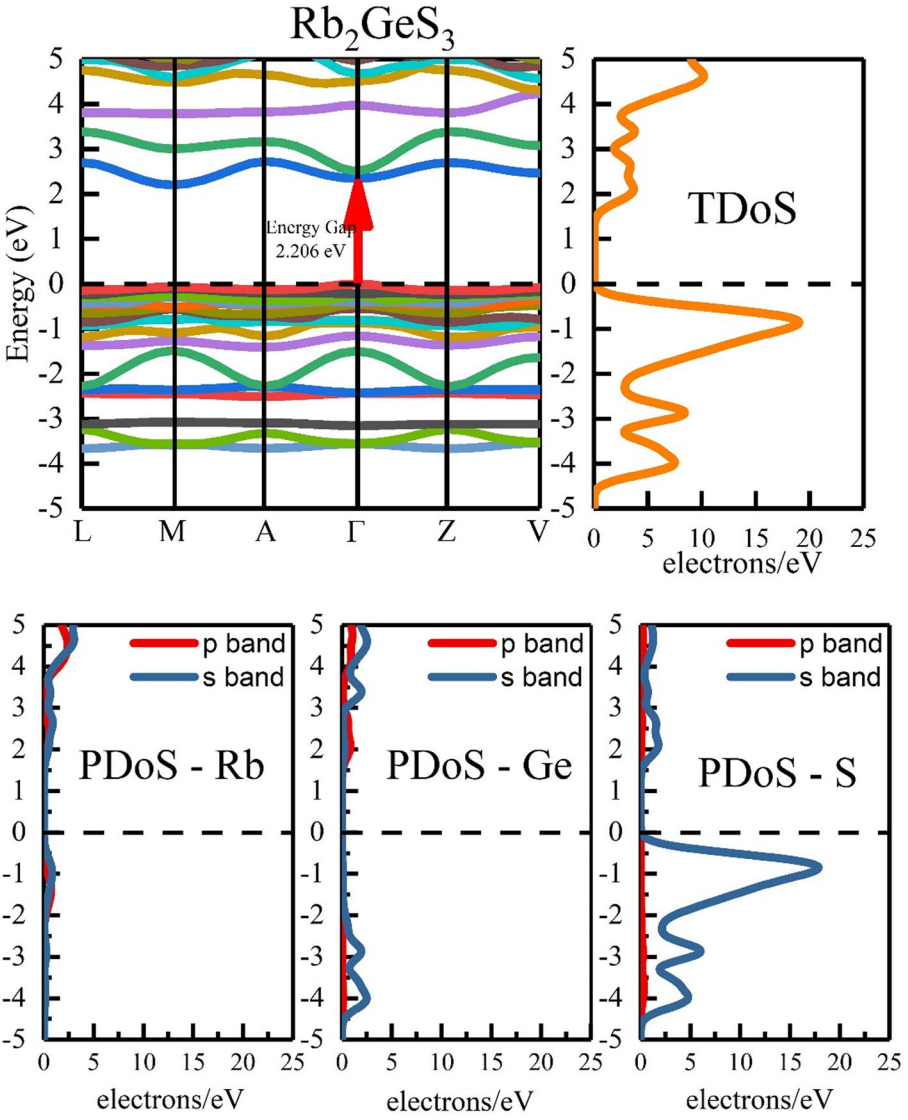


Fig. 3 Electronic band structure, total density of states, and partial density of state of Rb_2GeS_3

show the sharpest peaks at about 8 eV incident photon energies. So, this result supports their practical uses in functional UV applications (Bellil et al. 2021; Güler et al. 2021d, 2023b; Baaziz et al. 2022; Uğur et al. 2021a). In addition, refraction (n) and extinction(k) coefficients are two typical optic agents for applied optoelectronic technology. Figure 7 exhibits the (n) and (k) peaks of Rb_2XS_3 (X = Si, Ge, Sn) compounds deduced from: $n(\omega)=[(\varepsilon_1^2+\varepsilon_2^2)^{1/2}+\varepsilon_1)/2]^{1/2}$ and $k(\omega)=[(\varepsilon_1^2+\varepsilon_2^2)^{1/2}-\varepsilon_1)/2]^{1/2}$. In general, materials with $n>1.5$ are presumed to be high-refractors for manufacturing light-emitting diodes (LEDs) or organic light-emitting diodes (OLEDs) of contemporary optoelectronic tools. The calculated refractive indices (n) of Rb_2XS_3 (X = Si, Ge, Sn) compounds in Fig. 7, are over the

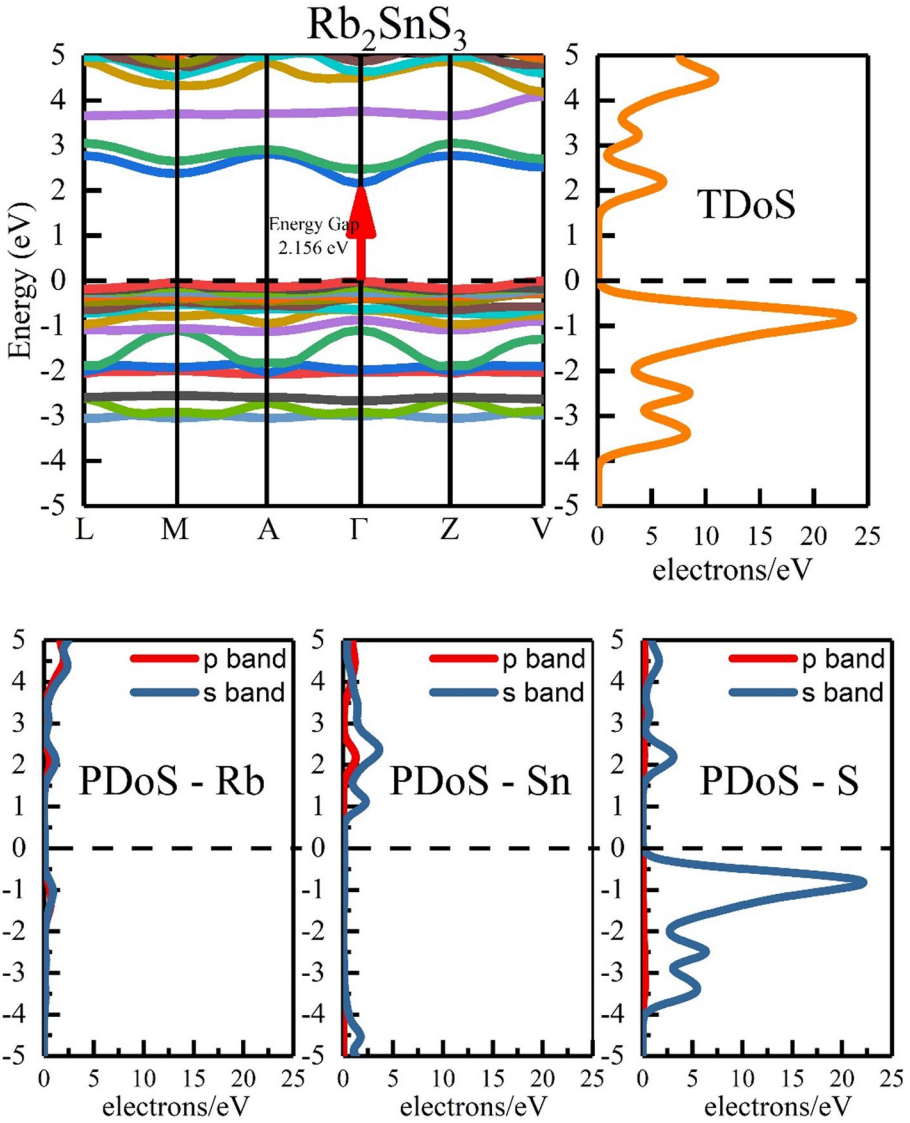


Fig. 4 Electronic band structure, total density of states, and partial density of state of Rb_2SnS_3

value of 2 and lie through the IR segment of the whole energy scale. Thus, Rb_2XS_3 (X = Si, Ge, Sn) compounds can be supposed to be new high-refractor alternatives for efficient IR purposes.

Figure 8 yields the absorption plots of Rb_2XS_3 (X = Si, Ge, Sn) compounds extracted from the equation $\alpha(\omega)=[\sqrt{2}\omega(\varepsilon_1^2+\varepsilon_2^2)^2-\varepsilon_1)^{1/2}]$. Strong light absorptions and oppositely weak optical reflections arise in semiconductors when the incoming energy of photons exceeds the bandgap energy values of the corresponding material. (Bellil et al. 2021; Güler et al. 2021d, 2023b; Baaziz et al. 2022; Uğur et al. 2021a). This trend is also valid

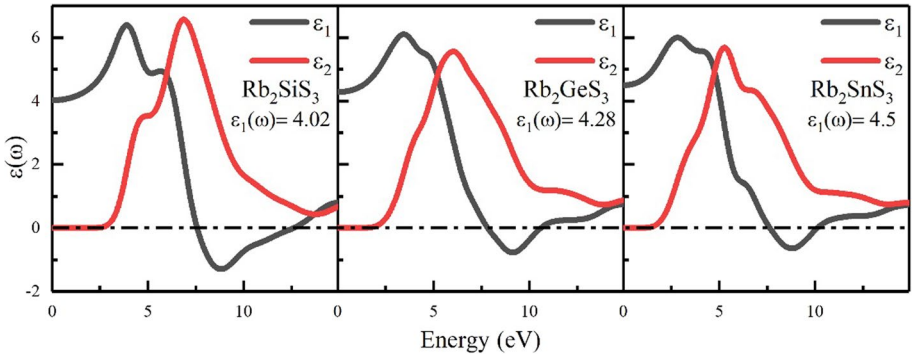


Fig. 5 Dielectric function of Rb_2SiS_3, Rb_2GeS_3 and Rb_2SnS_3

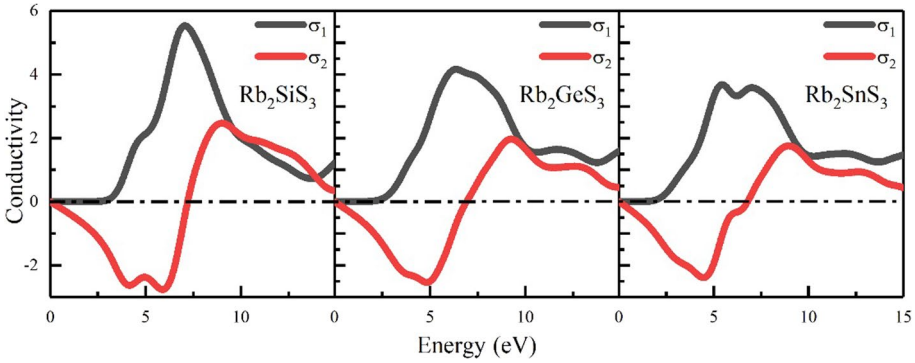


Fig. 6 Optical conductivity of Rb_2SiS_3, Rb_2GeS_3 and Rb_2SnS_3

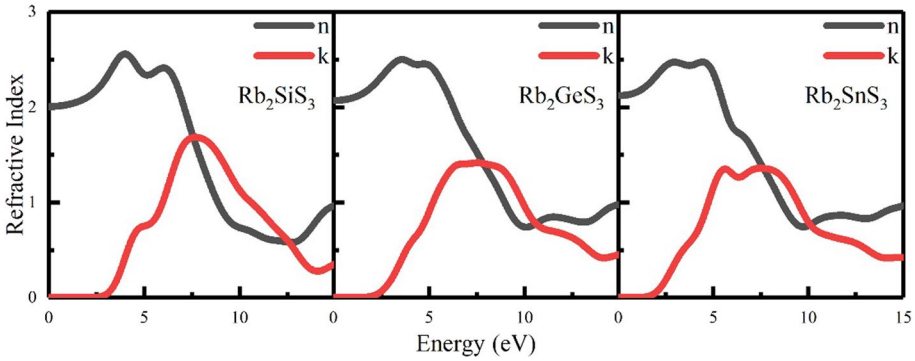


Fig. 7 Refractive index of Rb_2SiS_3, Rb_2GeS_3 and Rb_2SnS_3

for the studied Rb_2XS_3 (X = Si, Ge, Sn) compounds where the maximum absorptions for each compound remarkably emerge between 5 and 20 eV points of the UV in the range of $Rb_2SiS_3 > Rb_2GeS_3 > Rb_2SnS_3$ (Fig. 8). As another outcome, Rb_2XS_3 (X = Si, Ge, Sn)

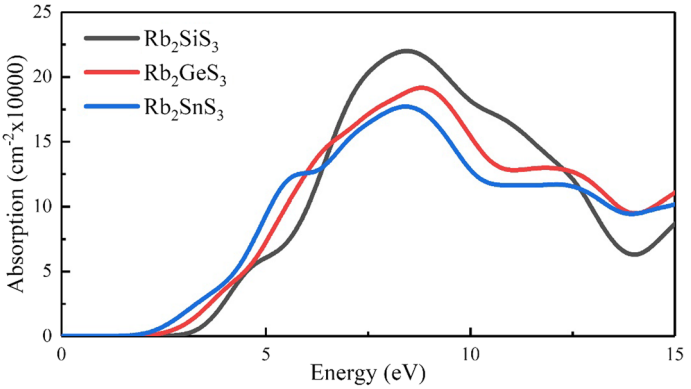


Fig. 8 Absorption plots of Rb_2SiS_3, Rb_2GeS_3 and Rb_2SnS_3

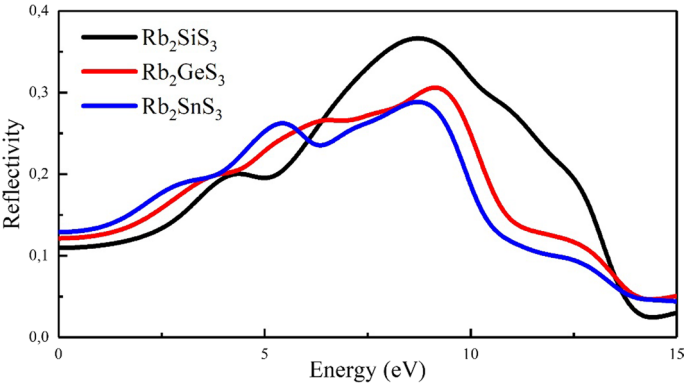


Fig. 9 Reflectivity of Rb_2SiS_3, Rb_2GeS_3 and Rb_2SnS_3

compounds may be regarded as capable absorbers and optical windows devices for feasible UV intents (Bellil et al. 2021; Güler et al. 2021d, 2023b; Baaziz et al. 2022; Uğur et al. 2021a).

Figure 9 also exposes the optical reflectance response of Rb_2XS_3 (X = Si, Ge, Sn) compounds concerning incident energy derived from the expression of R $(\omega) = [\{(n\text{-}1)^2 + k^2/(n+1)^2 + k^2\}]$ (Bellil et al. 2021; Güler et al. 2021d, 2023b; Baaziz et al. 2022; Uğur et al. 2021a). In Fig. 9, the reflection curves of Rb_2XS_3 (X = Si, Ge, Sn) compounds parade somewhat trivial reflectivity due to their strong absorption as described in the optical absorbance (Bellil et al. 2021; Güler et al. 2021d, 2023b; Baaziz et al. 2022; Uğur et al. 2021a).

The loss function parameter, acquired mostly from photon absorptions, stipulates knowledge of the energy loss of rapid inner electrons of materials (Bellil et al. 2021; Güler et al. 2021d, 2023b; Baaziz et al. 2022; Uğur et al. 2021a). The low-loss energy scales commonly occur amongst zero eV and 100 eV energy values, and characteristic sharp plasmon (joint vibrations of VB electrons) peaks exist at these energies. The loss plots in Fig. 10 depict the loss function behavior of Rb_2XS_3 (X = Si, Ge, Sn) compounds within the

adjusted photon energy pathway. As explicit in Fig. 10, it is possible to notice some energy loss in the small-scale energies around 12 eV for all compounds. Moreover, a specific plasmon peak releases at 23 eV for Rb_2SiS_3, where other compounds (Rb_2GeS_3 and Rb_2SnS_3) do not show the same characteristics. However, above 25 eV, loss function peaks of all surveyed compounds slightly decline to zero energy and conclusively reach the unity.

3.3 Obtained phonon dispersions and stability of Rb_2XS_3 (X = Si, Ge, Sn) compounds

The dynamic stability of materials is a significant issue for experimental synthesis and reliable production (Mouhat and Coudert 2014; Ye et al. 2018). So, it is worth checking the dynamical stability of any new material and deciding whether it is dynamically stable or not. At this point, phonon dispersions provide valuable knowledge about the stability of the materials of concern (Güler et al. 2022a, 2023c; Uğur et al. 2021b, 2023). For this reason, phonon dispersion curves of Rb_2XS_3 (X = Si, Ge, Sn) compounds were also addressed as an additional part of the present work to gain a piece of prior knowledge about the dynamical natures of Rb_2XS_3 (X = Si, Ge, Sn) compounds. Figure 11 renders the phonon dispersion plots of Rb_2XS_3 (X = Si, Ge, Sn) compounds obtained during this work. As detectible in Fig. 11, all phonon dispersion curves of Rb_2XS_3 (X = Si, Ge, Sn) compounds have positive (above zero) and definite frequency modes proving the evident dynamical stability (Güler et al. 2022a, 2023c; Uğur et al. 2021b, 2023) of the Rb_2XS_3 (X = Si, Ge, Sn) compounds. In other words, the presence of none imaginary phonon frequencies strongly underlines the dynamical stability of Rb_2XS_3 (X = Si, Ge, Sn) compounds, and these compounds can be easily synthesized from experiments to serve as alternative novel optoelectronic materials in demanding fields of the emergent technology.

3.4 Elastic properties and linking mechanical data of Rb_2XS_3 (X = Si, Ge, Sn) compounds

Clarifying elastic and interrelated mechanic data provides an in-depth understanding of a given material and handy predictions about the elastic and mechanical nature before production (Güler et al. 2022b; Güler and Güler 2014, 2015; Benmekideche et al. 2018;

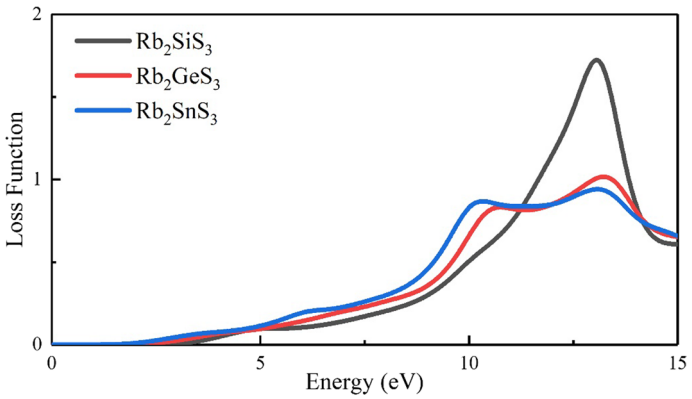


Fig. 10 Loss function of Rb_2SiS_3, Rb_2GeS_3 and Rb_2SnS_3

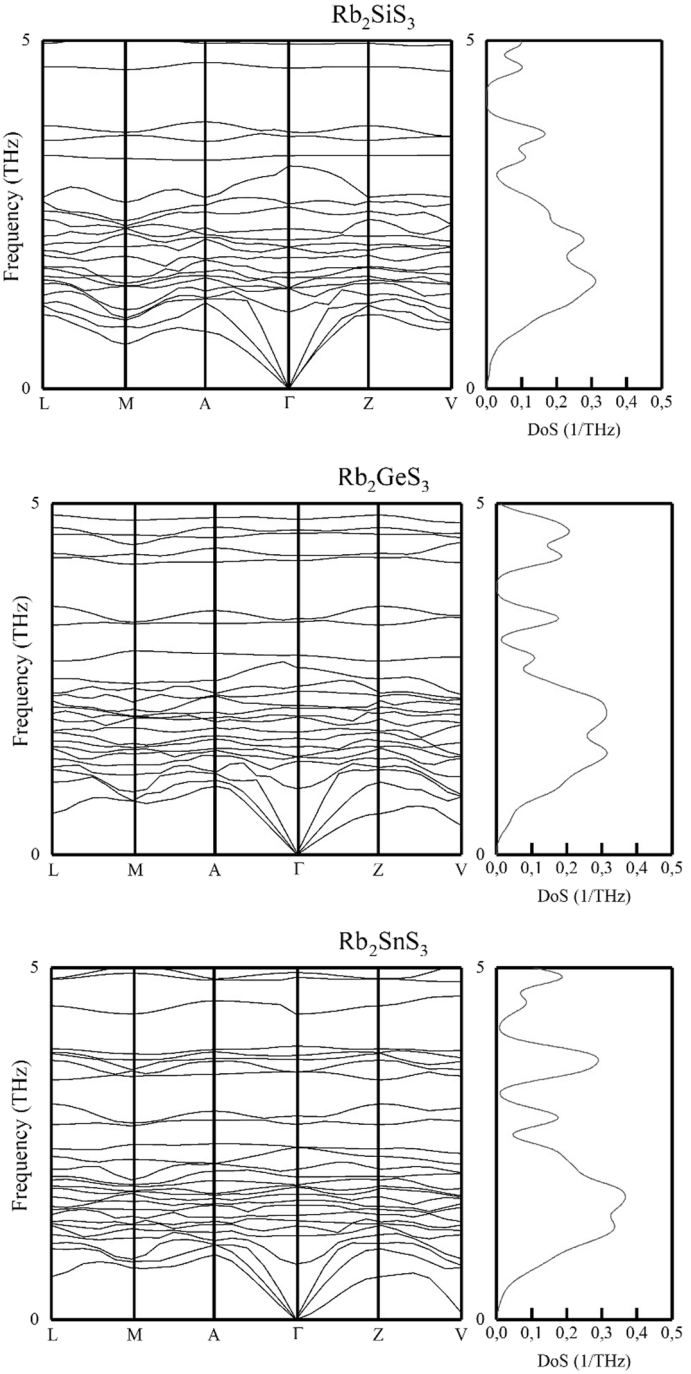


Fig. 11 Phonon dispersions and total density of states for Rb_2XS_3 (X = Si, Ge, Sn)

Živković et al. 2019; Naceur et al. 2022). So, as a result of these former predictions, it is possible to determine whether the examined material corresponds to the desired elastic and mechanical features. Under this focus, various elastic and connected mechanical data of Rb_2XS_3 (X = Si, Ge, Sn) compounds were also addressed and evaluated for the present work.

Elastic stiffness constants (C_{ij}) of materials are the most representative data of materials that decide the overall elastic and mechanical aspects of related materials. In this manner, since Rb_2XS_3 (X = Si, Ge, Sn) compounds monoclinic crystal structure, they yield 13 independent elastic constants due to their crystal symmetry (Güler et al. 2022b; Güler and Güler 2015, 2014; Benmekideche et al. 2018; Živković et al. 2019; Naceur et al. 2022), as readily summarized in Table 2. On the other hand, according to Born's mechanical stability norms, C_{ij} of the monoclinic systems must fulfill the requirements like; $C_{11} > 0$, $C_{22} > 0$, $C_{33} > 0$, $C_{44} > 0$, $C_{55} > 0$, $C_{66} > 0$, $C_{44}C_{66} - 2C_{46} > 0$, $C_{11} + C_{22} + C_{33} + 2(C_{12} + C_{13} + C_{23}) > 0$, $C_{22} + C_{33} - 2C_{23} > 0$ (Güler et al. 2022b; Güler and Güler 2014, 2015; Benmekideche et al. 2018; Živković et al. 2019; Naceur et al. 2022). So, from a mechanical stability outlook, currently computed Rb_2XS_3 (X = Si, Ge, Sn) compounds perform reliable mechanical stability due to the obtained corresponding data in Table 3. Several additional mechanical parameters derived from the elastic stiffness constants were also considered. For instance, the bulk modulus (B), shear (rigidity) modulus (G), and Young modulus (E) were also reported in Table 3 with Voigt-Reuss-Hill notations. From a mechanical aspect, B represents the internal resistance of materials to external deformations, whereas G denotes the response of the materials to the shear deformations. A material's Young modulus (E) (the modulus of elasticity), on the other hand, explains the material's stiffness subjected to a deformation along an axis when opposing forces are employed by this axis (Güler et al. 2022b; Güler and Güler 2015, 2014; Benmekideche et al. 2018; Živković et al. 2019; Naceur et al. 2022). As can be noticed in Table 3. the average Hill magnitudes of the bulk moduli of Rb_2XS_3 (X = Si, Ge, Sn) compounds track the $Rb_2SiS_3 > Rb_2GeS_3 > Rb_2SnS_3$ order where the same order is valid for the shear moduli and Young moduli of the investigated compounds. As another mechanical aspect, brittleness and ductility hold for two distinct and fundamental mechanical characteristics, particularly for the materials production process. Notably, easily broken brittle materials cannot be deformed much compared to more deformable and hardly broken ductile materials. At this stage, the Pugh ratio (B/G) is an important indicator of whether a material is brittle or ductile (Pingak et al. 2023; Joshi et al. 2021; Senkov and Miracle 2021). If $B/G > 1.75$, the material is ductile; otherwise,

Table 2 Calculated elastic constants C_{ij} (in GPa) of Rb_2XS_3 (X = Si, Ge, Sn)

C_{ij} (GPa)	Rb_2SiS_3	Rb_2GeS_3	Rb_2SnS_3
C_{11}	20.705	30.450	30.791
C_{22}	31.847	30.017	26.943
C_{33}	33.556	20.384	24.705
C_{44}	3.010	5.489	5.524
C_{55}	9.294	8.370	8.998
C_{66}	6.028	2.564	1.448
C_{12}	7.072	5.428	3.724
C_{13}	9.111	8.842	9.131
C_{23}	6.134	7.504	5.453
C_{46}	-0.415	-0.577	-1.178

Table 3 Calculated bulk modulus B (all in GPa), shear modulus G (all in GPa), Young's modulus E (all in GPa), Poisson's ratio ν and the B/G ratio of Rb_2XS_3 (X = Si, Ge, Sn)

Parameter	Rb_2SiS_3	Rb_2GeS_3	Rb_2SnS_3
B_V	14.527	13.822	13.228
B_R	13.987	13.518	13.007
B_H	14.257	13.670	13.118
G_V	7.919	7.223	7.469
G_R	6.084	5.394	3.668
G_H	7.002	6.309	5.569
E_V	20.105	18.455	18.859
E_R	15.942	14.284	10.058
E_H	18.051	16.403	14.635
ν	0.310	0.323	0.371
B/G	2.298	2.505	3.552

it is brittle (Pingak et al. 2023; Joshi et al. 2021; Senkov and Miracle 2021). Again, from Table 3, since all Pugh ratio values of the Rb_2XS_3 (X = Si, Ge, Sn) compounds are larger than the critical limit of 1.75, it is easy to conclude that all the surveyed compounds are ductile in nature where the highest value belongs to Rb_2SnS_3 with 3.55. As an additional mechanical parameter, Poisson's ratio (ν) shows how the cross-section of a deformable material varies under lengthwise stretching or compression. (Shah et al. 2023; Yoo et al. 2018; Zhang et al. 2023). It can also propose precious info about the brittle or ductile abilities of the relevant materials (Pius et al. 2023; Mott and Roland 2009). For example, $\nu < 0.26$ signifies the brittle materials, and $\nu > 0.26$ indicates the ductile capacity of regarding material (Pius et al. 2023; Mott and Roland 2009). The stated ν values of Rb_2XS_3 (X = Si, Ge, Sn) compounds in Table 3. with 0.31, 0.32, and 0.37, once more underline the ductile performance of Rb_2XS_3 (X = Si, Ge, Sn) compounds and confirms mutually the presently obtained Pugh ratio results (Table 3).

On the whole, compared to former theoretical work performed only for the bandgaps of Rb_2SiS_3 with 2.83 eV and Rb_2GeS_3 with 2.33 eV (Gorai et al. 2019), our results reported in this work for the same parameters for Rb_2SiS_3 with 2.806 eV and Rb_2GeS_3 with 2.206 eV are reasonable. Remarkably, although this work addresses a complimentary outlook including elastic, phonon and mechanical parameters of Rb_2XS_3 (X = Si, Ge, Sn) compounds, unfortunately there is no available data reported for the elastic, phonon and mechanical properties to conduct a complete comparison.

4 Conclusions

Hitherto, unreported electronic, optical, phonon, elastic, and mechanical features of Rb_2XS_3 (X = Si, Ge, Sn) semiconducting chalcogen compounds were analyzed and evaluated thanks to DFT computations. The main conclusions of the work can be given point by point as in the following:

- Obtained electronic band gaps with 2.806 eV for Rb_2SiS_3, 2.206 eV for Rb_2GeS_3 and 2.156 eV for Rb_2SnS_3 proves the semiconducting nature of these compounds.
- According to presently obtained optical dielectric constants data, all Rb_2XS_3 (X = Si, Ge, Sn) compounds can be good alternatives as high-k dielectric replacement materials

of recent silicon dioxide gate dielectrics frequently used in semiconductor technology and microelectronics.

- High optical conductivities make Rb_2XS_3 (X = Si, Ge, Sn) compounds ideal candidates for functional UV applications.
- Due to their materials with $n > 1.5$ are presumed to be high-refractors for manufacturing light-emitting diodes (LEDs) or organic light-emitting diodes (OLEDs) of contemporary optoelectronic tools.
- Because of their high refractive indexes over 2 along the IR region, Rb_2XS_3 (X = Si, Ge, Sn) compounds can also be promising materials for manufacturing light-emitting diodes (LEDs) or organic light-emitting diodes (OLEDs) and new high-refractor alternatives of efficient IR purposes.
- Since they have satisfactory optical absorbance characteristics, Rb_2XS_3 (X = Si, Ge, Sn) compounds may be regarded as capable absorbers and optical windows devices for feasible UV intents.
- All phonon dispersions for Rb_2XS_3 (X = Si, Ge, Sn) compounds yield positive frequencies denoting dynamical stability, suggesting the easy experimental synthesis of compounds. In addition, thermodynamic potentials of the reactions and their kinetic parameters of Rb_2XS_3 (X = Si, Ge, Sn) compounds should be also considered during further experiments to concretize this theoretical foresight obtained from the present phonon dispersions.
- Computed elastic stiffness constants prove the mechanical stability of all compounds.
- All compounds have a ductile nature attained from the mutual agreement of Pugh ratio analyses and calculated Poisson ratio values.

Author contributions ŞU, MG, AÖ, EG and GU have directly participated in the planning, execution, and analysis of this study. All authors have read and approved the final version of the manuscript.

Funding Open access funding provided by the Scientific and Technological Research Council of Türkiye (TÜBİTAK). The authors declare that no funds, grants, or other support were received during the preparation of this manuscript.

Data availability Data are available from the corresponding authors on reasonable request.

Declarations

Conflict of interest The authors have no relevant financial or non-financial interests to disclose.

Ethics approval Not applicable.

Consent for publication The authors confirm that there is informed consent to the publication of the data contained in the article.

Consent to participate Informed consent was obtained from all authors.

Open Access This article is licensed under a Creative Commons Attribution 4.0 International License, which permits use, sharing, adaptation, distribution and reproduction in any medium or format, as long as you give appropriate credit to the original author(s) and the source, provide a link to the Creative Commons licence, and indicate if changes were made. The images or other third party material in this article are included in the article's Creative Commons licence, unless indicated otherwise in a credit line to the material. If material is not included in the article's Creative Commons licence and your intended use is not

permitted by statutory regulation or exceeds the permitted use, you will need to obtain permission directly from the copyright holder. To view a copy of this licence, visit http://creativecommons.org/licenses/by/4.0/.

References

Azam, S., Irfan, M., Abbas, Z., Rani, M., Saleem, T., Younus, A., Akhtar, N., Liaqat B., Shabbir M., Al-Sehemi, Abdullah G.: DFT study of the electronic and optical properties of ternary chalcogenides AlX2Te4, Materials Research Express **6**, 116314 (2019). https://doi.org/10.1088/2053-1591/ab4b81

Baaziz, H., Ghellab, T., Güler, E., Charifi, Z., Uğur, Ş, Güler, M., Uğur, G.: Investigating the magnetic, mechanical, electronic, optical, and anisotropic properties of ZrCoFe X (X= Si, Ge) quaternary heusler alloys via first principles. J. Supercond. Nov. Magn. **35**, 1173–1182 (2022). https://doi.org/10.1007/s10948-022-06155-2

Bellil, N.B., Litimein, F., Khachai, H., Khenata, R., Abdiche, A., Güler, E., Ahmed, R., Bouhemadou, A., Omran, S.B., Khalifeh, J.M.: Structural, optoelectronic and thermodynamic characteristic of orthorhombic SnZrCH3 (CH= S, Se) compounds: insights from DFT computations. Mater. Today Commun. **27**, 102427 (2021). https://doi.org/10.1016/j.mtcomm.2021.102427

Benmekideche, N., Bentabet, A., Bouhadda, Y., Boubatra, D., Belgoumri, Gh., Fetah, S., Benmakhlouf, A., Benyelloul, K.: DFT study of structural, electronic and elastic properties of two polymorphs of monoclinic CsGaQ2 (Q= S, Se). Chin. J. Phys. **56**, 1345–1352 (2018). https://doi.org/10.1016/j.cjph.2018.03.006

Bennett, J.W.: Exploring the A2BX3 family for new functional materials using crystallographic database mining and first-principles calculations. J. Phys. Chem. C **124**, 19413–19425 (2020). https://doi.org/10.1021/acs.jpcc.0c03093

Clark, S.J., Segall, M.D., Pickard, C.J., Hasnip, P.J., Probert, M.I.J., Refson, K., Payne, M.C.: First principles methods using CASTEP, Zeitschrift für kristallographie-crystalline materials 220, 567–570 (2005). https://doi.org/10.1524/zkri.220.5.567.65075

Gorai, P., McKinney, R.W., Haegel, N.M., Zakutayev, A., Stevanovic, V.: A computational survey of semiconductors for power electronics. Energy Environ. Sci. **12**, 3338–3347 (2019). https://doi.org/10.1039/c9ee01529a

Güler, M., Güler, E.: Embedded atom method-based geometry optimization aspects of body-centered cubic metals. Chin. Phys. Lett. **30**, 056201 (2013). https://doi.org/10.1088/0256-307x/30/5/056201

Güler, E., Güler, M.: Phase transition and elasticity of gallium arsenide under pressure. Mat. Res. **17**, 1268–1272 (2014). https://doi.org/10.1590/1516-1439.272414

Güler, E., Güler, M.: Elastic and mechanical properties of cubic diamond under pressure. Chin. J. Phys. **53**, 040807 (2015). https://doi.org/10.6122/CJP.20141230

Güler, E., Güler, M., Uğur, Ş, Uğur, G.: First principles study of electronic, elastic, optical and magnetic properties of Rh2MnX (X = Ti, Hf, Sc, Zr, Zn) Heusler alloys. Int. J. Quantum Chem. **121**, e26606 (2021a). https://doi.org/10.1002/qua.26606

Güler, E., Güler, M., Uğur, Ş, Uğur, G.: DFT aspects of the elastic, mechanical, magnetic, thermodynamic and optical properties of Ce3XY perovskites. Phil. Mag. **102**, 244–263 (2021b). https://doi.org/10.1080/14786435.2021.1988172

Güler, M., Uğur, Ş, Uğur, G., Güler, E.: First principles study of the electronic, optical, elastic and thermoelectric properties of Nb2WNi alloy. Mol. Phys. **119**, e1928314 (2021c). https://doi.org/10.1080/00268976.2021.1928314

Güler, M., Güler, E., Uğur, Ş, Uğur, G., Charifi, Z., Baaziz, H.: Elastic, mechanical, anisotropic, optical and magnetic properties of V2NiSb Heusler alloy. Phys. Scr. **96**, 035807 (2021d). https://doi.org/10.1088/1402-4896/abdb54

Güler, E., Uğur, Ş, Güler, M., Özdemir, A., Uğur, G.: Revealing the electronic, optical, phonon and thermoelectrical characteristics of bulk and monolayered RbLiS and RbLiSe compounds by DFT. J. Phys. Chem. Solids **170**, 110972 (2022a). https://doi.org/10.1016/j.jpcs.2022.110972

Güler, E., Uğur, Ş, Güler, M., Uğur, G.: Exploring the elastic, mechanical and anisotropic response of Ti-5Al-XSn alloys through DFT calculations. Chin. J. Phys. **77**, 151–160 (2022b). https://doi.org/10.1016/j.cjph.2022.02.016

Güler, E., Uğur, Ş, Güler, M., Uğur, G.: Unveiling the electronic, optical, and thermoelectrical properties of bulk and monolayer AlSiTe3 by first principles. Chem. Phys. **575**, 112068 (2023a). https://doi.org/10.1016/j.chemphys.2023.112068

Güler, M., Uğur, Ş, Güler, E., Özdemir, A., Kuswaha, A.K., Genç, A.E., Uğur, G.: Investigating the electronic, elastic, mechanical, anisotropic, and optical aspects of Sc2RuZ (Z: Al, Ga, and In) full Heusler

alloys from the first principles. Physica B Condens. Matter. **659**, 414863 (2023b). https://doi.org/10.1016/j.physb.2023.414863
Güler, E., Güler, M., Özdemir, A., Genç, A.E., Uğur, G., Uğur, Ş: DFT predictions of the electronic, phonon, optical, and thermoelectric characteristics of CaCu2S2. MRS Commun. **13**, 1320–1325 (2023c). https://doi.org/10.1557/s43579-023-00463-x
Hoang, K., Mahanti, S.D.: Atomic and electronic structures of IV-VI2 ternary chalcogenides, J. Sci.: Adv. Mater. Devices. 1, 51–56 (2016). https://doi.org/10.1016/j.jsamd.2016.04.004
Jain, A., Ong, S.P., Hautier, G., Chen, W., Richards, W.D., Dacek, S., Cholia, S., Gunter, D., Skinner, D., Ceder, G., Persson, K.A.: Commentary: the materials project: a materials genome approach to accelerating materials innovation. APL Mater. **1**, 011002 (2013). https://doi.org/10.1063/1.4812323
Jawad, M., Rahman, A.U., Rafique, Q., Azam, S., Ijaz, F.: First principle investigation of structural, electronic, optical and thermoelectric properties of Chalcogenide Sr2GeX4 (X= S, Se). Mater. Sci. Semicond. Process. **173**, 108105 (2024). https://doi.org/10.1016/j.mssp.2023.108105
Joshi, H., Vu, T.V., Hieu, N.N., Khenata, R., Rai, D.P.: Mechanical and thermodynamical properties of Fe2CoAl a full-Heusler alloy under hydrostatic pressure: a DFT study. Mater. Chem. Phys. **270**, 124792 (2021). https://doi.org/10.1016/j.matchemphys.2021.124792
Khan, A.C., Cook, A.S., Leginze, J.A., Bennett, J.W.: Developing new antiferroelectric and ferroelectric oxides and Chalcogenides within the A2BX3 family. J. Mater. Res. **37**, 346–359 (2022). https://doi.org/10.1557/s43578-021-00410-3
Kirklin, S., Saal, J.E., Meredig, B., Thompson, A., Doak, J.W., Aykol, M., Rühl, S., Wolverton, C.: The open quantum materials database (OQMD): assessing the accuracy of DFT formation energies. Npj Comput. Mater. **1**, 15010 (2015). https://doi.org/10.1038/npjcompumats.2015.10
Kormath Madam Raghupathy, R., Wiebeler, H., Kühne, T.D., Felser, C., Mirhosseini, H.: Database screening of ternary chalcogenides for p-type transparent conductors. Chem. Mater. **30**, 6794–6800 (2018). https://doi.org/10.1021/acs.chemmater.8b02719
Lejaeghere, K., Van Speybroeck, V., Van Oost, G., Cottenier, S.: Error estimates for solid-state density-functional theory predictions: an overview by means of the ground-state elemental crystals. Crit. Rev. Solid State Mater. Sci. **39**, 1–24 (2013). https://doi.org/10.1080/10408436.2013.772503
Mbilo, M., Musembi, R.: First-principle calculations to investigate structural, electronic, elastic, mechanical, and optical properties of K2CuX (X=As, Sb) ternary compounds. Adv. Mater. Sci. Eng. **2022**, 1–10 (2022). https://doi.org/10.1155/2022/1440774
McKeever, H., Patil, N.N., Palabathuni, M., Singh, S.: Functional alkali metal-based ternary chalcogenides: design, properties, and opportunities. Chem. Mater. **35**, 9833–9846 (2023). https://doi.org/10.1021/acs.chemmater.3c01652
Monkhorst, H.J., Pack, J.D.: Special points for Brillouin-zone integrations. Phys. Rev. B **13**, 5188 (1976). https://doi.org/10.1103/PhysRevB.13.5188
Mott, P.H., Roland, C.M.: Limits to Poisson's ratio in isotropic materials. Phys. Rev. B **80**, 132104 (2009). https://doi.org/10.1103/physrevb.80.132104
Mouhat, F., Coudert, F.X.: Necessary and sufficient elastic stability conditions in various crystal systems. Phys. Rev. B **90**, 224104 (2014). https://doi.org/10.1103/physrevb.90.224104
Naceur, Y., Bourbaba, H., Ghebouli, M.A., Krache, L., Ghebouli, B., Chihi, T., Fatmi, M., Sultan, A.: Ab-initio study of structural, elastic, electronic and optical properties of hexahalometallate single crystals K2XBr 6 (X= Se, Pt). Sci. Rep. **12**, 8345 (2022). https://doi.org/10.1038/s41598-022-12570-1
Perdew, J.P., Burke, K., Ernzerhof, M.: Generalized gradient approximation made simple. Phys. Rev. Lett. **77**, 3865–3868 (1996). https://doi.org/10.1103/physrevlett.77.3865
Perdew, J.P., Burke, K., Ernzerhof, M.: Perdew Burke and Ernzerhof reply. Phys. Rev. Lett. **80**, 891 (1998). https://doi.org/10.1103/physrevlett.80.891
Pingak, R.K., Bouhmaidi, S., Harbi, A., Setti, L., Nitti, F., Moutaabbid, M., Johannes, A.Z., Hauwalie, N.U.J., Ndii, M.Z.: A DFT investigation of lead-free TlSnX 3 (X= Cl, Br, or I) perovskites for potential applications in solar cells and thermoelectric devices. RSC Adv. **13**, 33875–33886 (2023). https://doi.org/10.1039/d3ra06685a
Pius, K.K., Ongwen, N.O., Mageto, M., Odari, V., Gaitho, F.M.: Mechanical properties of Al–Mg–Si alloys (6xxx Series): a DFT-based study. Alloys **2**, 213–226 (2023). https://doi.org/10.3390/alloys2030015
Segall, M.D., Shah, R., Pickard, C.J., Payne, M.C.: Population analysis of plane-wave electronic structure calculations of bulk materials. Phys. Rev. B **54**, 16317–16320 (1996). https://doi.org/10.1103/physrevb.54.16317

Segall, M.D., Lindan, P.J.D., Probert, M.J., Pickard, C.J., Hasnip, P.J., Clark, S.J., Payne, M.C.: First-principles simulation: ideas, illustrations and the CASTEP code. J. Phys. Condens. Matter **14**, 2717 (2002). https://doi.org/10.1088/0953-8984/14/11/301

Senkov, O.N., Miracle, D.B.: Generalization of intrinsic ductile-to-brittle criteria by Pugh and Pettifor for materials with a cubic crystal structure. Sci. Rep. **11**, 4531 (2021). https://doi.org/10.1038/s41598-021-83953-z

Shah, M.A.H., Nuruzzaman, M., Hossain, A., Jubair, M., Zilani, M.A.K.: A DFT insight into structural, mechanical, elasto-acoustic, and anisotropic properties of AePdH3 (Ae= Ca, Sr, Ba) perovskites under pressure. Comput. Conden. Matter **34**, e00774 (2023). https://doi.org/10.1016/j.cocom.2022.e00774

Shen, C., Li, T., Zhang, Y., Xie, R., Long, T., Fortunato, N.M., Liang, F., Dai, M., Shen, J., Wolverton, C.M., Zhang, H.: Accelerated screening of ternary chalcogenides for potential photovoltaic applications. J. Am. Chem. Soc. **145**, 21925–21936 (2023). https://doi.org/10.1021/jacs.3c06207

Sujith, C.P., Joseph, S., Mathew, T., Mathew, V.: Exploring the electronic and optical anisotropy of quasi-one-dimensional ternary chalcogenide CrSbSe3: a DFT study. Solid State Sci. **130**, 106926 (2022). https://doi.org/10.1016/j.solidstatesciences.2022.106926

Uğur, Ş, Güler, M., Uğur, G., Güler, E.: Elastic, mechanical, optical and magnetic properties of Ru2MnX (X= Nb, Ta, V) Heusler alloys. J. Magn. Magn. Mater. **523**, 167614 (2021a). https://doi.org/10.1016/j.jmmm.2020.167614

Uğur, G., Kushwaha, A.K., Güler, M., Charifi, Z., Uğur, Ş, Güler, E., Baaziz, H.: Electronic structure, optical and vibrational properties of Ti2FeNiSb2 and Ti2Ni2InSb double half heusler alloys. Mater. Sci. Semicond. Process. **123**, 105531 (2021b). https://doi.org/10.1016/j.mssp.2020.105531

Uğur, Ş, Güler, E., Güler, M., Özdemir, A., Uğur, G.: Analyzing the electronic and optical properties of bulk, unstrained, and strained monolayers of SrS2 by DFT. Phys. E: Low-Dimens. Syst. Nanostructures **143**, 115403 (2022). https://doi.org/10.1016/j.physe.2022.115403

Uğur, G., Güler, M., Uğur, Ş, Güler, E.: DFT exploration of the electronic, optical, phonon and thermoelectrical performances of bulk and monolayered AuCN. Theor. Chem. Acc. **142**, 20 (2023). https://doi.org/10.1007/s00214-023-02960-7

Wang, Q., Ma, H., Ni, B., Li, Y., Huang, S., Lin, W., Zhang, Y.: Validation of density functional theory methods for predicting the optical properties of cu-based multinary chalcogenide semiconductors. J. Phys. Chem. C **126**, 4684–4697 (2022). https://doi.org/10.1021/acs.jpcc.1c10510

Ye, W., Chen, C., Wang, Z., Chu, I.-H., Ong, S.P.: Deep neural networks for accurate predictions of crystal stability. Nat. Commun. **9**, 3800 (2018). https://doi.org/10.1038/s41467-018-06322-x

Yoo, Y., Yang, J.H., Lee, J.H.: First-principles study on the Poisson's ratio of transition-metal dichalcogenides. Curr. Appl. Phys. **18**, 799–802 (2018). https://doi.org/10.1016/j.cap.2018.03.018

Zhang, L., Jiao, F., Qin, W., Wei, Q.: New insight into elastic mechanical properties and anisotropies of crystal defect α-Quartz from DFT calculation. ACS Omega **8**, 43644–43650 (2023). https://doi.org/10.1021/acsomega.3c05173

Živković, A., Farkaš, B., Uahengo, V., de Leeuw, N.H., Dzade, N.Y.: First-principles DFT insights into the structural, elastic, and optoelectronic properties of α and β-ZnP2: implications for photovoltaic applications. J. Phys. Condens. Matter **31**, 265501 (2019). https://doi.org/10.1088/1361-648x/ab111c

Publisher's Note Springer Nature remains neutral with regard to jurisdictional claims in published maps and institutional affiliations.